

# Identifying Patterns and Sources of Fine and Ultrafine Particulate Matter in London Using Mobile Measurements of Lung-Deposited Surface Area

Rishabh U. Shah,\* Lauren E. Padilla, Daniel R. Peters, Megan Dupuy-Todd, Elizabeth R. Fonseca, Geoffrey Q. Ma, Olalekan A. M. Popoola, Roderic L. Jones, Jim Mills, Nicholas A. Martin, and Ramón A. Alvarez



Cite This: *Environ. Sci. Technol.* 2023, 57, 96–108



Read Online

ACCESS |

Metrics & More

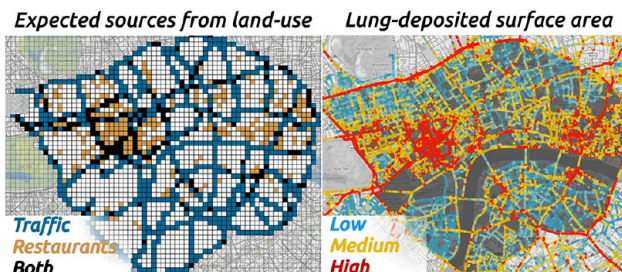
Article Recommendations

Supporting Information

**ABSTRACT:** We performed more than a year of mobile, 1 Hz measurements of lung-deposited surface area (LDSA, the surface area of 20–400 nm diameter particles, deposited in alveolar regions of lungs) and optically assessed fine particulate matter ( $\text{PM}_{2.5}$ ), black carbon (BC), and nitrogen dioxide ( $\text{NO}_2$ ) in central London. We spatially correlated these pollutants to two urban emission sources: major roadways and restaurants. We show that optical  $\text{PM}_{2.5}$  is an ineffective indicator of tailpipe emissions on major roadways, where we do observe statistically higher LDSA, BC, and  $\text{NO}_2$ . Additionally, we find pollutant hot spots in commercial neighborhoods with more restaurants. A low LDSA ( $15 \mu\text{m}^2 \text{cm}^{-3}$ ) occurs in areas with fewer major roadways and restaurants, while the highest LDSA ( $25 \mu\text{m}^2 \text{cm}^{-3}$ ) occurs in areas with more of both sources. By isolating areas that are higher in one source than the other, we demonstrate the comparable impacts of traffic and restaurants on LDSA. Ratios of hyperlocal enhancements ( $\Delta \text{LDSA}: \Delta \text{BC}$  and  $\Delta \text{LDSA}: \Delta \text{NO}_2$ ) are higher in commercial neighborhoods than on major roadways, further demonstrating the influence of restaurant emissions on LDSA. We demonstrate the added value of using particle surface in identifying hyperlocal patterns of health-relevant PM components, especially in areas with strong vehicular emissions where the high LDSA does not translate to high  $\text{PM}_{2.5}$ .

**KEYWORDS:** urban air quality, hyperlocal mapping, particulate matter, restaurant emissions, traffic emissions

## Mobile hyperlocal air quality measurements in London



## INTRODUCTION

Ambient fine particulate matter ( $\text{PM}_{2.5}$ , particles with an aerodynamic diameter of  $<2.5 \mu\text{m}$ ) is robustly associated with the global increase in conditions such as heart disease, stroke, and lung disease, leading to premature mortality.<sup>1–3</sup> While  $\text{PM}_{2.5}$  is typically measured, reported, and regulated using the proxy of mass concentration,  $\text{PM}_{2.5}$  samples with the same mass concentrations can have very different particle size distributions (illustrated in Figure S1), shapes, and chemical compositions, depending on their source and airborne age,<sup>4</sup> resulting in potentially very different health effects.<sup>5,6</sup> Ultrafine particles (UFPs, typically defined as particles with a diameter of  $<100 \text{ nm}$ ) are generally shown to have more adverse health effects because of their absorption into the bloodstream and translocation to vital organs.<sup>7,8</sup>

Because of their small diameter, UFPs are minor contributors of mass but dominant contributors of number and surface concentrations. For example, Ye et al.<sup>9</sup> and Apte et al.<sup>10</sup> have shown that while average intracity variations in mass concentrations are only 1.5–2 times the background levels,

these variations represent large average variations in number concentrations (7–10 times the background levels). In addition, due to rapid dilution and coagulation occurring over time scales of a few minutes,<sup>11</sup> the highest number concentrations occur largely near emission sources such as traffic and cooking<sup>10,12,13</sup> and decrease rapidly with distance from the source.<sup>14,15</sup> For example, Saha et al.<sup>16</sup> showed that with an increase in distance from a major roadway, particle number concentrations decrease dramatically ( $\Delta \sim -80\%$  at 200 m from highway), compared to particle mass ( $\Delta \sim -30\%$ ). Hence, identification of these hyperlocal enhancements (“hot spots”) of UFPs requires high-spatial resolution

Received: November 1, 2022

Revised: December 6, 2022

Accepted: December 6, 2022

Published: December 22, 2022



monitoring, which can be achieved either by a dense network of stationary sensors or by mobile monitoring.

Mobile monitoring has provided great insight into urban hot spots and sources of primary air pollutants, including PM<sub>2.5</sub>, UFPs, oxides of nitrogen (NO<sub>x</sub> = NO + NO<sub>2</sub>), carbon monoxide (CO), and black carbon (BC).<sup>10,17–23</sup> In addition, the emergence of low-cost air pollution sensors in the past decade, particularly low-cost optical PM sensors,<sup>24,25</sup> has significantly boosted the amount of spatially dense air pollution monitoring around the world, especially in highly polluted areas in low-income regions.<sup>26–33</sup> While increased spatial coverage is a tremendous benefit of low-cost sensors, the greatest challenge with their use compared to advanced, research-grade instrumentation is that of data quality arising from issues such as signal nonlinearity, noise, poor limits of detection and quantitation, sensor bias and drift, and interference from environmental conditions.<sup>24</sup> Another particular challenge involved with optical PM sensors is that the primary mode of detection is the amount of light scattered by a population of particles, which is then converted to mass concentration using empirical assumptions of properties such as particle morphology, refractive index, and density.<sup>24,34</sup> As a result, an optical PM sensor calibrated against a gravimetric reference instrument for one type of particle population (e.g., urban background, where the mode particle diameter is in the range of 0.5–2  $\mu\text{m}$ ) may not perform well when measuring a plume of smaller, freshly emitted particles. Finally, a crucial limitation of optical PM sensors is that due to their diameter detection limits, <300 nm particles (low-cost sensors) or <180 nm particles (reference-grade sensors) are not detected.<sup>24,35</sup> As a result, while optical PM sensors can be used to detect primary, coarse-mode PM emissions (>1  $\mu\text{m}$ , e.g., brake and tire wear, construction dust, etc.), they likely only partially detect particles in fresh cooking emissions (typically ~200 nm<sup>9</sup>) and likely do not detect particles in fresh engine exhaust emissions (typically ~30 nm<sup>9</sup>) at all.

Instead of the PM<sub>2.5</sub> mass, particle number and surface area measurements have been reported in the literature as a more effective proxy for detecting hyperlocal hot spots of fresh particle concentrations, geolocating their sources, and assessing exposures.<sup>36–39</sup> While the number concentration is the commonly measured approximation of UFPs in the literature, the particle surface area has been shown to be an important determinant for the toxicological influence of particulate matter, likely because surface chemistry is the primary mechanism of the interaction between particles and pulmonary tissue cells.<sup>6,40,41</sup> The metric most commonly used to report particle surface concentrations is lung-deposited surface area (LDSA, expressed in units of square micrometers per cubic centimeter), which is the total surface area of particles that could be deposited in the alveolar region of the human respiratory system (20–400 nm diameter range). While many previous high-spatial resolution monitoring studies have measured NO, NO<sub>2</sub>, BC, and particle mass concentrations,<sup>17–19,42–45</sup> relatively fewer studies have measured particle number concentrations,<sup>36–38,46</sup> and far fewer studies have measured LDSA.<sup>47–53</sup> Additionally, while the studies that reported non-LDSA measurements employed mobile monitoring, the LDSA measurements were all stationary, largely a few weeks to months long, and thus useful in ascertaining only temporal variations at the sampling location (e.g., urban background, indoors in an industrial facility, etc.). Given the crucial health relevance of LDSA as described above, the lack

of mobile, high-resolution measurements of LDSA in an urban area is a key gap in the scientific literature.

In this study, we address this gap by presenting mobile, high-spatial resolution, repeated, on-road measurements of LDSA in central London, along with simultaneous measurements of optically measured PM<sub>2.5</sub> mass, BC mass, and NO<sub>2</sub> mixing ratios. These measurements were conducted as part of the first year-long mobile air monitoring campaign in central London.<sup>54,55</sup> The large data set generated from repeated, year-long mobile measurements of these pollutants enables us to prepare high-resolution maps of long-term central tendencies of individual pollutant concentrations, as well as statistical analyses of uncertainty, local enhancements, interspecies ratios of enhancements, and, finally, spatial correlations between these metrics and two ubiquitously occurring urban particulate sources: major roadways and restaurants (land-use covariate proxies for vehicular and cooking emissions, respectively). To the best of our knowledge, this is the first study reporting high-spatial resolution, year-long, mobile measurements of LDSA. While our measurements represent on-road air pollution levels, we know from the literature that urban sources such as traffic and restaurants impact air quality over spatial scales of 100–500 m.<sup>16,20</sup> As such, the information about hyperlocal and neighborhood-scale variability derived from our measurements is relevant to off-road air quality receptors, as well. With more scientific attention going toward characterizing sources, concentrations, patterns, exposures, and acute and chronic health effects of particulate matter in urban environments, this study presents novel, relevant, and valuable findings using measurements of LDSA, a proxy for components of particulate matter with direct, toxicological implications.

## METHODS

**Data Collection.** We retrofitted two Google Street View (GSV) vehicles with identical suites of fast-response (1 Hz) pollutant measuring instruments. We used these vehicles to perform repeated measurements of pollutant concentrations from September 2018 to October 2019 on the major public roads of central London (of the total 407 km of roads in central London, our vehicles drove on 391 km at least once and on 335 km at least five times throughout the campaign) (Figure 1). Our drivers drove the vehicles predominantly on weekdays from 5 a.m. to 11 p.m., as shown in section S4 of the Supporting Information. When not sampling, the vehicles were parked at the National Physical Laboratory (NPL) in the Teddington suburb outside of central London, to connect with dedicated air conditioning systems to maintain the temperature control of the monitoring instruments and to allow periodic calibration of instruments, as described in our openly accessible documentation [this document also contains a detailed description of the quality assurance protocols employed for flagging mobile data for possible erroneous interference, uncertainty in position data, warmup periods, etc. (<https://www.globalcleanair.org/breathe-london-appendix-3-mobile-monitoring-documentation/>)].

**Instrumentation.** We measured LDSA using a Naneos Partector aerosol dosimeter, which uses a unipolar diffusion charger to distribute charges on particle surfaces. The resulting electric current generated by the flow of charged particles is measured with an electrometer and subsequently converted to LDSA using their known theoretical proportionality.<sup>56,57</sup> As described in the technical documentation for this sensor

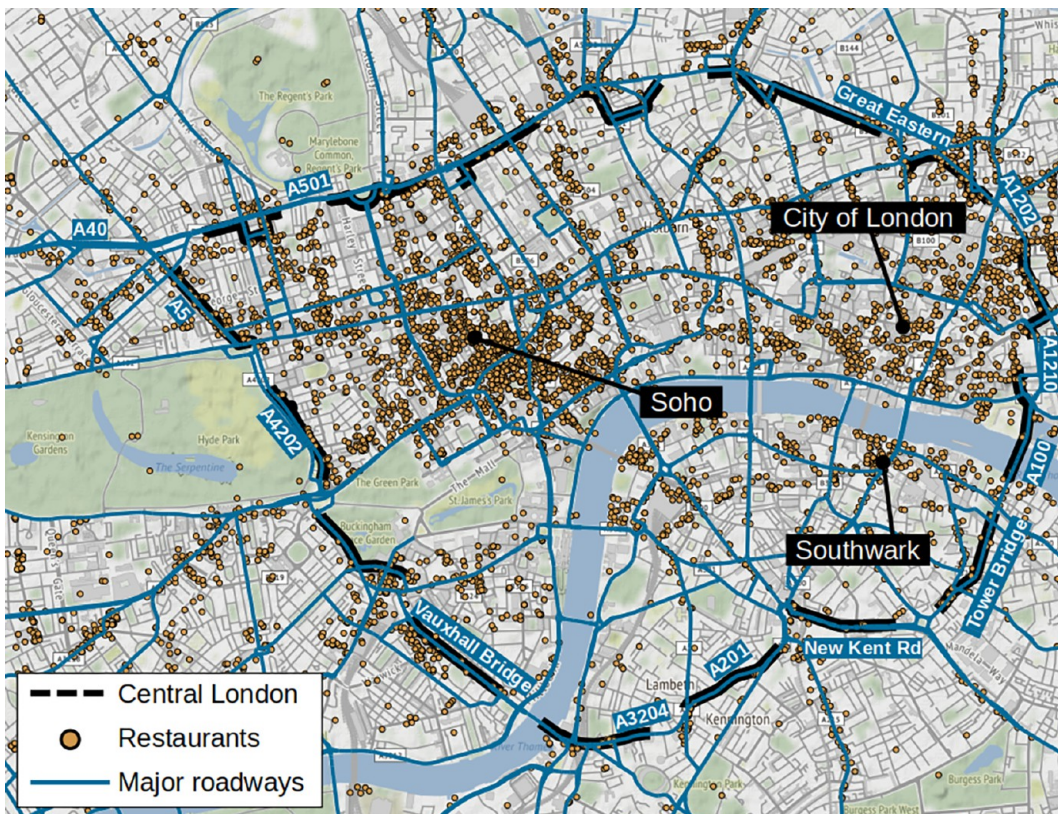


**Figure 1.** Sampling domain of this study: central London (indicated by the thick, dashed border). Solid lines indicate major roadways (motorways and primary arterial roads; e.g., the confines of central London are defined by the A501 at the northern border, the A5, A202, A302, and A4202 at the western border, the A3204, A201, and New Kent Road at the southern border, and Tower Bridge Road, A100, A1210, and Commercial Street at the eastern border), and circles show restaurant locations. Commercial areas of Soho, City of London, and Southwark have a particularly high density of restaurants. Map data by Stamen Design, under CC BY 3.0. Data by OpenStreetMap, under ODbL.

(accessible online at <https://www.naneos.ch/pdf/LDSA.pdf>), this proportionality constant is  $d^{-1.1}$ . This approach has been shown to report the surface area of particles between 20 and 400 nm accurately.<sup>58,59</sup>

We measured PM<sub>2.5</sub> using a Palas Fidas, a MCERTS-certified (Monitoring Certification Scheme, Environment Agency of England and Wales<sup>60</sup>) ambient fine dust measurement instrument. Briefly, ambient particles are dried prior to entering the optical counting chamber, where the amount of light scattered by each individual particle is measured and converted to particle size using principles of Lorenz–Mie light scattering. Thus, particles are counted and size-resolved into 64 logarithmically spaced size channels between 180 nm and 18  $\mu\text{m}$  (particles outside this size range are not detected). Additionally, the instrument's internal software converts these size-resolved particle counts into mass by relying on empirical assumptions of particle density. Finally, the mass distribution is integrated and recorded as PM<sub>2.5</sub>.

We measured BC and NO<sub>2</sub> using a Magee Scientific Aethalometer (AE33) and an Aerodyne cavity-attenuated phase shift monitor, respectively. Both of these instruments have been used in several previous studies.<sup>61–64</sup> Aethalometric measurements conducted at a high time resolution (1 Hz) have been shown to have a significant occurrence of negative values (e.g., >30%), especially when sampling at low concentrations.<sup>65</sup> Simply discarding these negatives is an inappropriate action to take, as this would bias the final data high because of positive fluctuations in the noise. Following Brantley et al.,<sup>62</sup> we smoothed the raw BC time series using a

10 s moving average filter. We acknowledge that this smoothing will result in a coarser spatial resolution for the filtered BC data. However, the primary focus of this study is on LDSA measurements, and we use BC as only a qualitative indicator of vehicular emissions<sup>42</sup> and not to derive quantitative metrics such as emission factors and health risks. In addition, when using BC data to infer source impacts, we also use NO<sub>2</sub> measurements as a co-emitted marker of vehicular emissions, thereby not relying solely on our BC data.

Our assessments of instrument performance and data quality are described in section S2.

**Data Reduction.** The quality control and quality assurance protocols (e.g., identifying and flagging erroneous data, adjusting timestamps of data for tubing residence time, i.e., nominal time taken by sample to traverse flow tubing and reach instruments) applied to our data are described in detail in our openly accessible documents (<https://www.globalcleanair.org/breathe-london-appendix-3-mobile-monitoring-documentation/>). We applied a data reduction methodology following Miller et al.<sup>19</sup> and Messier et al.<sup>66</sup> Briefly, we first split all roads into segments with a nominal length of 30 m, resulting in ~13 000 segments inside central London. We then attached each 1 Hz sample to the nearest 30 m road segment on the basis of recorded GPS coordinates. Next, for each road segment, we grouped individual samples into “drive passes”, i.e., 1 Hz samples collected consecutively while the vehicle was within the road segment. The purpose of defining drive passes is to avoid skewing each road segment's final central tendency toward a period when the vehicle spent

more time at the segment (e.g., due to slow-moving traffic). Next, for each road segment, all drive pass averages occurring within the same hour were grouped and averaged as a “drive period”. Finally, for each road segment, different drive periods from the entire measurement period were aggregated, and their median was used as the campaign median pollutant concentration for that segment. Because measurements spanned slightly more than a year (13 months), this campaign median can also be treated as the annual daytime median for the road segment.

### Identifying Local Enhancements and Emission Ratios.

Conceptually, the time series of pollutant concentrations acquired from a continuous mobile monitoring drive can be considered a combination of two components: (a) rapidly changing recent contributions from local sources, superimposed on top of (b) a temporally changing background concentration. This temporally varying background contribution could be from a spatially invariant, regional background, or in the case of mobile sampling, it could also be an intermediate, neighborhood-scale background, e.g., when the GSV car drives along a suburban-to-street-canyon-to-suburban transect. To identify local enhancements, we employed an enhancement identification method following Padilla et al.<sup>54</sup> Briefly, for each 1 Hz observation, a “background” concentration is identified (first percentile of the observations in the 150 s before and 150 s after; at a typical speed of 30 km h<sup>-1</sup>, this translates to a distance of just <2.5 km). Next, the difference between the total concentration and the background is defined as a local enhancement ( $\Delta$ ). Finally, these enhancements are filtered to account for instrument noise; i.e., if enhancements are larger than instrument noise, they are retained, but if they are not, they are discarded. For example, this filtering resulted in approximately 6% of  $\Delta$ LDSA and 9% of  $\Delta$ PM<sub>2.5</sub> samples being discarded. This background subtraction and enhancement identification process is illustrated in section S3. While this approach of identifying enhancements in pollutant time series has been used in previous studies,<sup>54,67,68</sup> it should be noted that these observed enhancements indicate the combined effect of various factors (e.g., number of sources, distance between the source and sampling point, and amounts of dispersion, dilution, mixing, etc., occurring in the interim) and thus should not be used to directly infer source properties, e.g., emission factors.

We further utilized contemporaneous enhancements of LDSA, PM<sub>2.5</sub>, BC, and NO<sub>2</sub> to calculate emission ratios and infer possible sources. Ratios of  $\Delta$ LDSA to  $\Delta$ PM<sub>2.5</sub>,  $\Delta$ BC, and  $\Delta$ NO<sub>2</sub> are used to infer whether the observed enhancement is from one of two possible sources: (a) locally emitted vehicular exhaust pollution (i.e., higher  $\Delta$ LDSA: $\Delta$ PM<sub>2.5</sub> ratio because of the large population of sub-100 nm, large-surface area, low-mass particles, with lower  $\Delta$ LDSA: $\Delta$ BC and  $\Delta$ LDSA: $\Delta$ NO<sub>2</sub> ratios due to co-emission of BC and NO<sub>2</sub>) and (b) nonvehicular emissions (e.g., cooking, which would presumably have lower  $\Delta$ LDSA: $\Delta$ PM<sub>2.5</sub> ratios because of the large population of ~200 nm particles that can be optically detected by the Fidas PM<sub>2.5</sub> monitor, and higher  $\Delta$ LDSA: $\Delta$ BC and  $\Delta$ LDSA: $\Delta$ NO<sub>2</sub> ratios<sup>12,36</sup>).

**Probability of Exceedance.** This methodology is described in detail by Padilla et al.<sup>54</sup> and described here briefly. Because only two GSVs performed sampling within the 22 km<sup>2</sup> central London region, sampling coverage can be sparse on some roads (section S5). As a result, the campaign median pollutant concentration estimated from mobile data at

each road segment will have an uncertainty that is influenced by the number of drive periods at that segment.<sup>17</sup> For each road segment, we estimated the sampling uncertainty in LDSA concentration as a function of the number of drive periods at that segment. Analyses of sampling uncertainty are described in the section S5. In addition, we incorporated the LDSA sensor uncertainty of  $\pm 30\%$ , as stated in its technical documentation, into our total LDSA uncertainty. With an increasing number ( $n$ ) of samples, this sensor uncertainty decreases by a factor of  $1/\sqrt{n}$ .

Thus, instead of representing each road segment by a single median concentration, we incorporate the segment’s total uncertainty to build a probability distribution about the segment’s median LDSA concentration. This enables us to calculate the probability that the median LDSA concentration at a road segment would exceed a certain threshold. We set this threshold to 25  $\mu\text{m}^2 \text{cm}^{-3}$  for LDSA and 10  $\mu\text{g m}^{-3}$  for PM<sub>2.5</sub>, which are approximately the 75th percentile of the city-wide distributions shown in Figure 2.

**Land-Use Classification.** We explored the spatial correlation between observed pollutant concentrations and two major urban sources: commercial kitchens (restaurants) and traffic (major roadways). Following Gu et al.,<sup>42</sup> we gridded the central London domain into 100 m  $\times$  100 m cells. We obtained locations of restaurants and roads within the domain by using the Yelp and OpenStreetMaps (OSM) application programming interfaces, respectively. Within each 100 m  $\times$  100 m grid cell, we calculated two land-use variables: restaurant count and length of major roadways (i.e., listed as either “motorway” or “primary” in the OSM database). The distributions of these variables are shown in Figure S17. In addition to analyzing these land-use metrics as continuous variables, we also used thresholds of  $\geq 4$  restaurants and  $\geq 20$  m of major roadways to classify each grid cell as “high” or “low” with respect to the two sources, consistent with Gu et al.<sup>42</sup> (These arbitrary thresholds are meant to compare only the pollution patterns in areas impacted by certain source types from others and are not meant to be used as determinant parameters of pollution concentrations, e.g., land-use regression models. While a more robust classification could be performed using sophisticated cluster analysis methods, e.g.,  $k$ -means clustering, they are beyond the scope of this study.) Of the 2266 total 100 m  $\times$  100 m grid cells, 235 are classified as “high restaurants, low traffic”, 691 are classified as “low restaurants, high traffic”, 198 are classified as “high restaurants, high traffic”, and the remaining 1142 are classified as “low source” (shown in Figure S17). Finally, we coupled this grid with our observed median pollutant concentrations at each road segment, and within each grid cell, we calculated the weighted average of the median pollutant concentration, where weights were the lengths of road segments falling inside the grid cell. For instance, the median pollutant concentration ( $C$ ) for a 100 m  $\times$  100 m grid cell is a function of the campaign median concentration,  $m$ , and the length,  $l$ , of each of the  $n$  30 m road segments contained within the cell:

$$C = \frac{\sum_{i=1}^n m_i l_i}{\sum_{i=1}^n l_i} \quad (1)$$

## RESULTS AND DISCUSSION

In this section, we present spatial and temporal patterns of campaign median pollutant concentrations using various

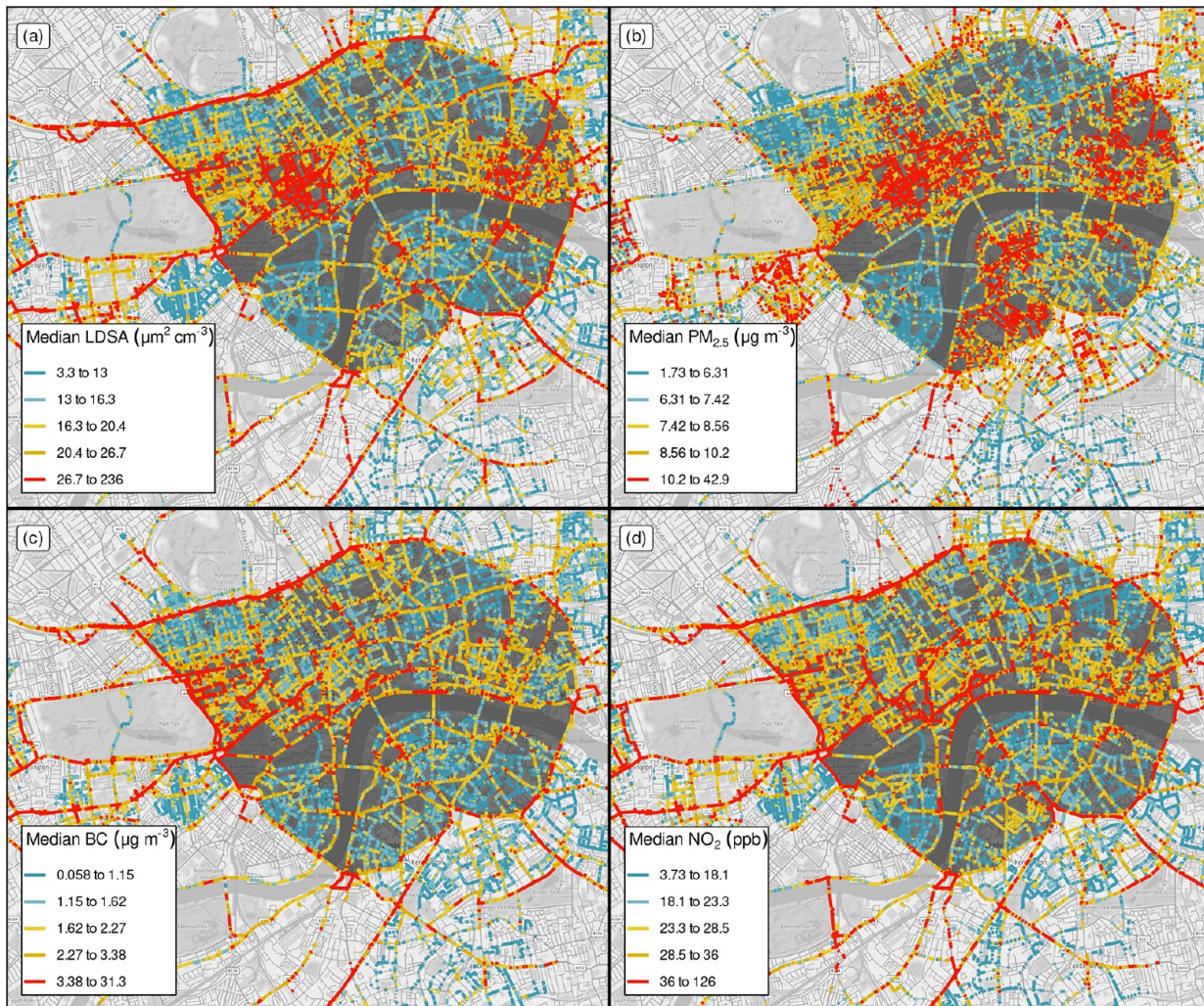


**Figure 2.** Campaign median absolute concentrations of (a) LDSA, (b) PM<sub>2.5</sub>, (c) BC, and (d) NO<sub>2</sub> at 30 m road segments. In each pollutant map, the five colors represent natural breaks; i.e., each color represents 20 quantiles. Road segments with fewer than five drives are not shown. The central London region is shown with the dark gray backdrop. Map data by Stamen Design, under CC BY 3.0. Data by OpenStreetMap, under ODbL.

analyses performed at the 30 m road segment level: (1) absolute pollutant concentrations, (2) diurnal behavior of campaign median concentrations, (3) local enhancements and interpollutant enhancement ratios, (4) probability of exceedance, and (5) gridded correlations between pollutant concentrations and land-use covariates.

**Absolute Pollutant Concentrations.** Figure 2 shows the absolute, campaign median concentrations of LDSA, PM<sub>2.5</sub>, BC, and NO<sub>2</sub> at 30 m road segments. Instead of a continuous color ramp, we categorize the concentrations into five natural quantiles so as to show the distribution of the road segments. For instance, the city-wide campaign median concentration is approximately the midpoint of the third level, i.e., approximately 18  $\mu\text{m}^2 \text{cm}^{-3}$  for LDSA, 8  $\mu\text{g m}^{-3}$  for PM<sub>2.5</sub>, 2  $\mu\text{g m}^{-3}$  for BC, and 27 ppb for NO<sub>2</sub>. In comparison to other LDSA measurement studies, the London LDSA levels shown here are more similar to urban background measurements in Leicester (22  $\mu\text{m}^2 \text{cm}^{-3}$ ) and Zürich (19  $\mu\text{m}^2 \text{cm}^{-3}$ )<sup>48,53</sup> than to more polluted areas such as Barcelona (37  $\mu\text{m}^2 \text{cm}^{-3}$ )<sup>49</sup>, Lisbon (34  $\mu\text{m}^2 \text{cm}^{-3}$ )<sup>69</sup>, and Los Angeles (53  $\mu\text{m}^2 \text{cm}^{-3}$ )<sup>52</sup>.

In addition, the lower bounds of the second and fifth color levels indicate the 20th and 80th percentiles of the distribution

( $p_{20}$  and  $p_{80}$ ), respectively, and thus, the difference between  $p_{20}$  and  $p_{80}$  (a proxy for the spread of the distribution) indicates the spatial variability for the pollutant. The spatial variability for LDSA is 13.7  $\mu\text{m}^2 \text{cm}^{-3}$  (75% of the city-wide median), while those for PM<sub>2.5</sub>, BC, and NO<sub>2</sub> are 3.9  $\mu\text{g m}^{-3}$  (49% of the city-wide median), 2.2  $\mu\text{g m}^{-3}$  (114% of the city-wide median), and 17.9 ppb (69% of the city-wide median), respectively. The observed order of spatial variability (BC > LDSA > NO<sub>2</sub> > PM<sub>2.5</sub>), qualitatively consistent with other urban mobile sampling studies,<sup>10,16,17</sup> likely occurs because BC and LDSA are predominantly primary, more nonconserved pollutants while NO<sub>2</sub>, and especially PM<sub>2.5</sub>, are relatively more conserved pollutants (illustrated in section S6). The term “conserved” is used here following the definition of conserved and nonconserved pollutants as described by Apte et al.<sup>10</sup> Nonconserved pollutants are those that decay on time scales that are as fast or faster than the air transit time from emission site to ambient receptor, and thus, increments in these pollutant concentrations are good geographic tracers of their sources. Conserved pollutants such PM<sub>2.5</sub>, on the contrary, have substantial regional background contributions, and thus,

near-source concentrations are only moderately increased above the regional background levels.

The maps in Figure 2 show different areas of the city having persistently increased concentrations of different pollutants. LDSA, for instance, is higher on the major roadways inside, bordering, and outside central London. LDSA is also higher in the commercial areas in Soho, City of London, and Southwark. In contrast,  $\text{PM}_{2.5}$  is higher in the commercial neighborhoods, but not on any of the major roadways with high LDSA.  $\text{PM}_{2.5}$  is apparently also higher in the southwestern portion of central London; however, this is likely an artifact resulting from sampling bias, as discussed later and evidenced in section S8. BC and  $\text{NO}_2$ , both indicators of traffic emissions, are increased almost exclusively on major roadways. This is particularly evident in the Soho neighborhood, where BC and  $\text{NO}_2$  are increased on the three major roadways, but not in other parts of the neighborhood, whereas LDSA is increased in the entire neighborhood. This difference in behavior between observed spatial patterns of different pollutants can likely be explained by two hypotheses. First, increments of LDSA, BC, and  $\text{NO}_2$  occur on major roadways due to vehicle exhaust emissions. Freshly emitted vehicular exhaust particles, being smaller than 100 nm,<sup>9</sup> were likely not detected by our optical  $\text{PM}_{2.5}$  sensor (lower diameter cutoff of 180 nm). Second, the neighborhood-scale LDSA and  $\text{PM}_{2.5}$  hot spots in commercial areas occur due to emissions containing particles larger than this cutoff of 180 nm. One such possibility is that of non-exhaust vehicular emissions such as brake wear, tire wear, and road dust resuspension, which are in the far coarser diameter range (often  $>1 \mu\text{m}$ ).<sup>70,71</sup> Congestion of traffic in commercial areas would, for instance, result in stop-and-go behavior of vehicles, leading to increased brake wear emissions. However, it would be reasonable to expect that vehicular non-exhaust emissions would be co-emitted with observable exhaust emissions of  $\text{NO}_2$ . Another possibility is that of the influence of particles in cooking emissions, which are shown to be between 100 and 400 nm in diameter.<sup>9</sup> The dense presence of restaurants in commercial areas has been shown to be an important contributor and determinant for such neighborhood-scale enhancements in particulate matter.<sup>14,18,20,72,73</sup>

**Diurnal Behavior.** To explore the hypotheses presented in the previous section, we stratified our LDSA concentrations into four diurnal time periods: morning (5 a.m. to 10 a.m.), midday (10 a.m. to 2 p.m.), afternoon (2 p.m. to 7 p.m.), and evening (7 p.m. to midnight). We use these four time periods to distinguish the effects of vehicular emissions (which would be more pronounced in the morning and afternoon periods) from cooking emissions (which would be more pronounced during midday and evening). The campaign median LDSA concentrations in these four diurnal periods are shown in section S7. In the morning period, major roadways exhibit increased LDSA, which is likely explained by peak commuter traffic at this time. While the Soho commercial area exhibits only mild increments of LDSA along its main roads in the morning, it exhibits increased LDSA on local or minor roadways during the midday period. This effect is even more pronounced in the commercial neighborhoods in the evening period. While stratifying the data into time periods introduces additional statistical uncertainty into quantifying concentrations at the 30 m scale (as explained in the accompanying text in the section S7), the observed diurnal behavior is qualitatively consistent with the hypotheses that vehicular sources increase LDSA concentrations on major roadways and

restaurants increase LDSA in commercial neighborhoods. The hypothesis of the impact of cooking emissions on ambient LDSA levels is also consistent with the finding presented in the study by Hama et al.,<sup>48</sup> who found increased LDSA levels during weekends at an urban background site in Leicester, U.K., and attributed this enhancement to cooking emissions from barbecue activities and overall increased commercial activity.

### Local Enhancements and Interpollutant Emission Ratios.

To distinguish the effect of local, primary emissions from that of temporal variations in urban background concentrations, we calculated a background-subtracted component of recorded concentrations (denoted as  $\Delta$ ).

Overall, the spatial patterns observed after background subtraction are similar to the corresponding absolute concentration maps shown in Figure 2. Hence, we show campaign median concentrations of only  $\Delta\text{LDSA}$  in Figure 3, while we show similar maps for  $\Delta\text{PM}_{2.5}$ ,  $\Delta\text{BC}$ , and  $\Delta\text{NO}_2$  in Figure S14.  $\Delta\text{LDSA}$  is higher on major roadways and in commercial areas;  $\Delta\text{BC}$  and  $\Delta\text{NO}_2$  are prominent on major roadways, while  $\Delta\text{PM}_{2.5}$  is higher in commercial areas. Because only  $\Delta$  values larger than instrument noise were saved as valid enhancements and only road segments with five or more observed valid enhancements are shown in these maps, there are several blank spaces on these maps compared to the maps shown in Figure 2. The road segments that are displayed in Figure 3 and Figure S14 despite these filters are thus those where these enhancements are frequent.

Previously, we argued that the higher spatial variability of BC and LDSA compared to that of  $\text{NO}_2$  and  $\text{PM}_{2.5}$  was because the former two are predominantly primary, non-conserved pollutants while the latter two (especially  $\text{PM}_{2.5}$ ) are relatively more conserved pollutants; i.e., near-source concentrations are often only mildly increased above larger regional background levels.<sup>10,17</sup> This point is further corroborated in the spatial variability of background-subtracted enhancements shown in Figure 3 and Figure S14. The widths of these distributions ( $p_{80} - p_{20}$ ), in decreasing order, are  $11 \mu\text{m}^2 \text{cm}^{-3}$  for LDSA (153% of the city-wide median),  $2.3 \mu\text{g m}^{-3}$  for BC (98% of the city-wide median), 13.3 ppb for  $\text{NO}_2$  (85% of the city-wide median), and  $1.7 \mu\text{g m}^{-3}$  for  $\text{PM}_{2.5}$  (30% of the city-wide median). It is thus evident that of these four pollutants,  $\text{PM}_{2.5}$  is the most conserved pollutant, and thus the poorest tracer of primary emissions because of the important contribution and spatial invariance of its secondary components. For instance, the  $\text{PM}_{2.5}$  map in Figure 2 shows the southern portion of central London as one of the neighborhoods having a high campaign median  $\text{PM}_{2.5}$  concentration. However, Figure S14 shows that  $\Delta\text{PM}_{2.5}$  does not exhibit this behavior, suggesting that this apparent increment in absolute  $\text{PM}_{2.5}$  is likely an artifact resulting from regional background levels being higher on days when this neighborhood was visited for sampling. As shown in Figure S15, our estimated background  $\text{PM}_{2.5}$  indeed agrees well with stationary measurements as reported by urban background monitors of the London Air Quality Network. While ultrafine particle number and LDSA levels have been shown to be impacted by meteorological processes in other locations (e.g., new particle formation from regional nucleation),<sup>48,74</sup> we find that background LDSA levels in London are quite stable below  $10 \mu\text{m}^2 \text{cm}^{-3}$ , even during high ozone and high  $\text{NO}_2:\text{NO}_x$  periods when nucleation would be most expected (Figure S8).

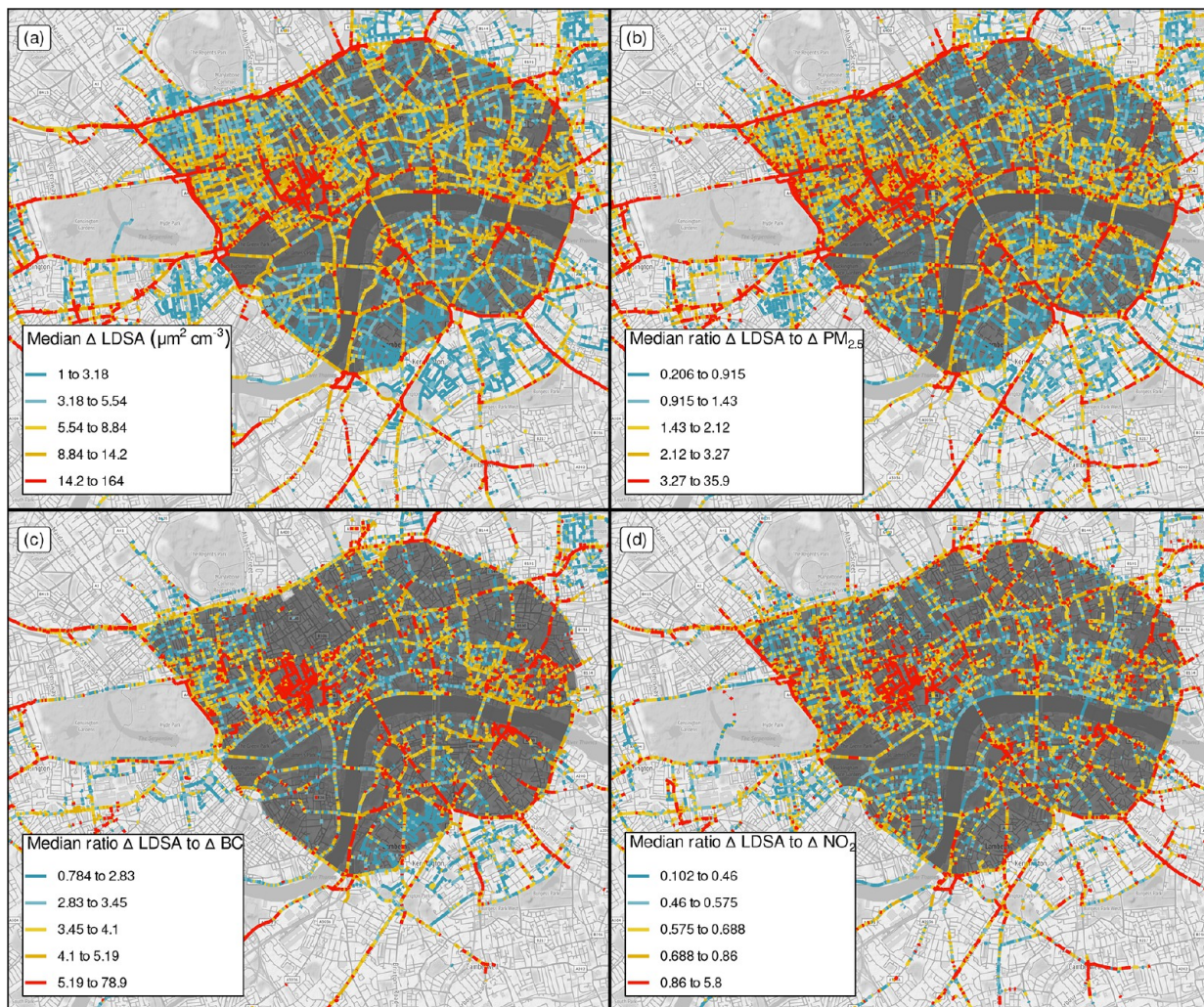


**Figure 3.** (a) Campaign median concentrations of background-subtracted ( $\Delta$ ) LDSA. (b–d) Campaign median interpollutant emission ratios:  $\Delta \text{LDSA:}\Delta \text{PM}_{2.5}$  in units of  $(\mu\text{m}^2 \text{ cm}^{-3})/(\mu\text{g m}^{-3})$ ,  $\Delta \text{LDSA:}\Delta \text{BC}$  in units of  $(\mu\text{m}^2 \text{ cm}^{-3})/(\mu\text{g m}^{-3})$ , and  $\Delta \text{LDSA:}\Delta \text{NO}_2$  in units of  $(\mu\text{m}^2 \text{ cm}^{-3})/\text{ppb}$ . In each pollutant map, the five colors represent natural quantiles; i.e., the number of road segments in each category is the same. Road segments with fewer than five observed enhancements are not shown. The central London region is shown with the dark gray backdrop. Map data by Stamen Design, under CC BY 3.0. Data by OpenStreetMap, under ODbL.

This is consistent with the literature showing few occurrences of nucleation and new particle formation in London.<sup>75,76</sup>

In addition to calculating enhancements of individual pollutants, we also analyzed contemporaneous enhancements of multiple pollutants to calculate interpollutant emission ratios. In Figure 3, we show three maps for campaign median emission ratios:  $\Delta \text{LDSA:}\Delta \text{PM}_{2.5}$ ,  $\Delta \text{LDSA:}\Delta \text{BC}$ , and  $\Delta \text{LDSA:}\Delta \text{NO}_2$ . These ratios further indicate the possible effect of different sources on observed plume strengths. For instance,  $\Delta \text{LDSA:}\Delta \text{PM}_{2.5}$  being higher on major roadways (e.g., the A501 major roadway at the northern edge of central London) is consistent with the aforementioned explanation that fresh vehicular exhaust emissions are measured in LDSA, but likely not in  $\text{PM}_{2.5}$  (because of the optical size cutoff of 180 nm of our Fidas monitor, but also generally because fresh exhaust particles do not contribute much mass<sup>10</sup>). Further evidence of this is the fact that  $\Delta \text{LDSA:}\Delta \text{BC}$  and  $\Delta \text{LDSA:}\Delta \text{NO}_2$  are lower on these major roadways (because of higher  $\Delta \text{BC}$  and  $\Delta \text{NO}_2$  from vehicle exhaust emissions, which is consistent with Lepisto et al.<sup>77</sup>) and higher in the

Soho commercial district, where cooking emissions are likely more abundant.

**Probability of Exceedance.** To account for sampling uncertainty caused by sparse sampling coverage on certain 30 m road segments, we built probability distributions of the road segments' campaign median LDSA concentrations. Thus, instead of calculating just the campaign median concentration at a road segment, we calculated the probability that the median there will exceed a certain threshold. We set this threshold to  $25 \mu\text{m}^2 \text{ cm}^{-3}$ , which is approximately the 75th percentile of the city-wide distribution shown in Figure 2. Figure 4 shows these probabilities of exceedance.

In the two maps shown in Figure 4, high exceedance probabilities occur on road segments where one of these conditions is met: (a) The estimated campaign median concentration is higher than the threshold of  $25 \mu\text{m}^2 \text{ cm}^{-3}$ , such that this exceedance is captured despite an insufficient number of samples. (b) The estimated campaign median concentration is only slightly higher than the threshold, but this exceedance is likely captured because of the large number of samples. (c) The estimated campaign median concentration

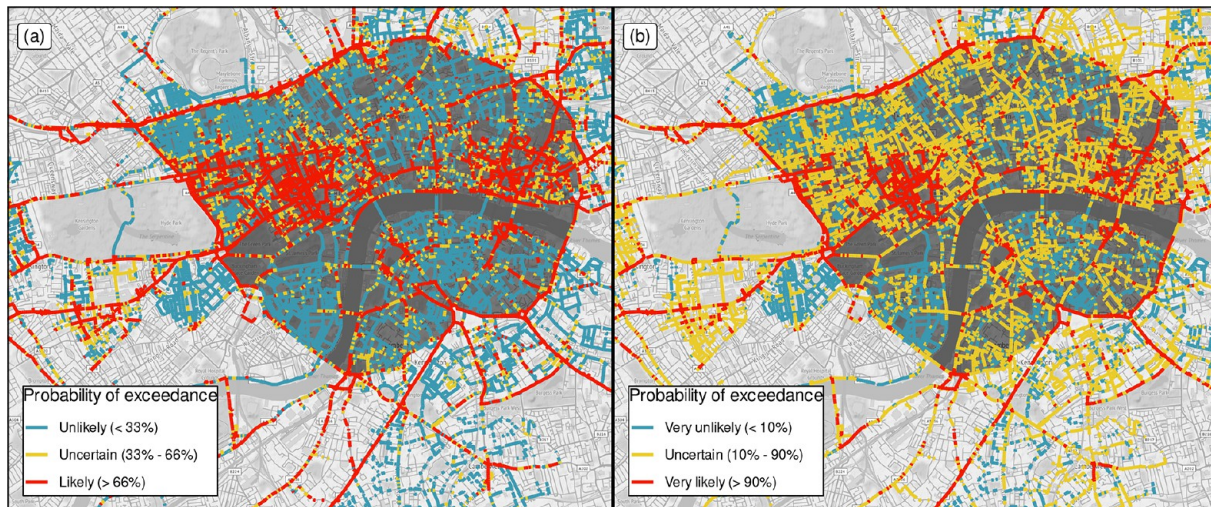


**Figure 4.** Probability of exceedance applied to LDSA data. On the basis of each road segment's probability distribution, it is classified into one of three categories of exceedance with respect to the city-wide 75th percentile concentration of  $25 \mu\text{m}^2 \text{ cm}^{-3}$ . These limits for this classification are set equally in map a, i.e., each probability class is 33% wide, and more strictly in map b, i.e., unless highly certain to either exceed or not, segments are classified as uncertain. Map data by Stamen Design, under CC BY 3.0. Data by OpenStreetMap, under ODbL.

is well over the threshold, and the number of samples is also large enough to build additional confidence (the third condition is the most desirable target of mobile monitoring, but due to uneven sampling coverage, this is also an ideality). **Figure 4** shows that the major roadways (e.g., A5, A501, A4202, and A100) and the commercial areas of Soho, City of London, and Southwark are likely ( $>66\%$  probability) to exceed the LDSA threshold of  $25 \mu\text{m}^2 \text{ cm}^{-3}$ . With the exception of City of London, these hot spots are also found to be very likely ( $>90\%$  probability) to exceed this threshold.

Similar probability of exceedance maps for  $\text{PM}_{2.5}$  are shown in **Figure S16**. For  $\text{PM}_{2.5}$ , we set the threshold to  $10 \mu\text{g m}^{-3}$ , which is approximately the 75th percentile of the city-wide distribution in **Figure 2**. Incidentally, unlike our LDSA threshold of  $25 \mu\text{m}^2 \text{ cm}^{-3}$ , our threshold of  $10 \mu\text{g m}^{-3}$  has meaningful significance because this was also the World Health Organization guideline for healthy annual average exposure prior to September 22, 2021. **Figure S16** shows that  $\text{PM}_{2.5}$  is unlikely to exceed on any of the major roadways where LDSA is likely to exceed.  $\text{PM}_{2.5}$  is likely, but not very likely, to exceed on many road segments in the commercial areas of Soho, City of London, and Southwark (i.e., probability of exceedance between 66% and 90%). In fact, it is only in central Soho and some parts of City of London where  $\text{PM}_{2.5}$  is found to be very likely to exceed  $10 \mu\text{g m}^{-3}$ .

**Gridded Correlations between Pollutant Concentrations and Land-Use Covariates.** **Figure 5** shows the distributions of gridded campaign median LDSA concentrations within each grid group. The “low-source” grid group has the lowest LDSA concentrations (median of  $15 \mu\text{m}^2 \text{ cm}^{-3}$ ); the high restaurant, low traffic (HR-LT) and low restaurant, high traffic (LR-HT) groups have statistically similar medians of  $\sim 20 \mu\text{m}^2 \text{ cm}^{-3}$ , and finally, the high restaurant, high traffic (HR-HT) group has a higher median of  $\sim 25 \mu\text{m}^2 \text{ cm}^{-3}$ . Consistent with the literature,<sup>16,18,42</sup> the observed order of concentrations across these grid groups demonstrates the comparable and additive nature of traffic and restaurant PM emissions. Similar plots for  $\text{PM}_{2.5}$ , BC, and  $\text{NO}_2$  are shown in **Figure S19**. For both BC and  $\text{NO}_2$ , the LR-HT and HR-HT grid groups are statistically similar to each other

(median BC of  $\sim 2.5 \mu\text{g m}^{-3}$ , median  $\text{NO}_2$  of  $\sim 30 \text{ ppb}$ ) and are higher than the “low-source” and HR-LT groups (median BC of  $\sim 1.6 \mu\text{g m}^{-3}$ , median  $\text{NO}_2$  of  $\sim 22 \text{ ppb}$ ), demonstrating the prominent effect of traffic emissions from major roadways on these species, while the presence of restaurants has little additional effect. It should be noted that median BC and  $\text{NO}_2$  for the HR-LT grid group, while only  $\sim 0.15 \mu\text{g m}^{-3}$  and  $\sim 3 \text{ ppb}$  higher, respectively, are still found to be statistically higher than those of the low-source grid group, likely because of the additional traffic emissions on local roads in commercial areas.

As discussed above, fresh vehicular exhaust emissions of  $\text{PM}_{2.5}$  are likely largely missed by our Fidas monitor, while cooking emissions (with a larger median diameter) should be at least partially captured. This effect is demonstrated in **Figure S19**, where the HR-LT and HR-HT grid groups are statistically similar (median  $\text{PM}_{2.5}$  of  $\sim 8.8 \mu\text{g m}^{-3}$ ) and higher by  $\sim 1 \mu\text{g m}^{-3}$  compared to the low-source and LR-HT groups.

In addition to gridding the campaign medians of absolute pollutant concentrations, we also applied these analyses to background-subtracted enhancements and interpollutant emission ratios. **Figure 5** also shows the gridded ratio of  $\Delta\text{LDSA}$  to  $\Delta\text{PM}_{2.5}$ . While absolute LDSA concentrations are similar for the HR-LT and LR-HT groups,  $\Delta\text{LDSA}:\Delta\text{PM}_{2.5}$  is higher in the LR-HT group than in the HR-LT group. This shows that our observed LDSA and  $\text{PM}_{2.5}$  concentrations are correlated and co-emitted in the cells with high restaurant counts, but in areas of high traffic, observed  $\Delta\text{LDSA}$  concentrations are higher than  $\Delta\text{PM}_{2.5}$ , causing this ratio to be higher. Other similar plots of background-subtracted enhancements and interpollutant ratios are shown in **Figures S21 and S23**. The overall behavior and comparison between grid groups remain consistent with the explanations presented earlier. Strong markers of vehicular exhaust emissions ( $\Delta\text{BC}$  and  $\Delta\text{NO}_2$ ) are higher in high-traffic grid groups (HR-HT and LR-HT), while  $\Delta\text{LDSA}$ , a marker of both traffic and restaurant emissions, is higher in all grid groups other than the low-source group. Interestingly, while LDSA concentrations were similar for HR-LT and LR-HT groups,  $\Delta\text{LDSA}$  is higher for the LR-HT group than for the HR-LT group, likely because enhancements result from fresh vehicular emissions of sub-100 nm particles, which

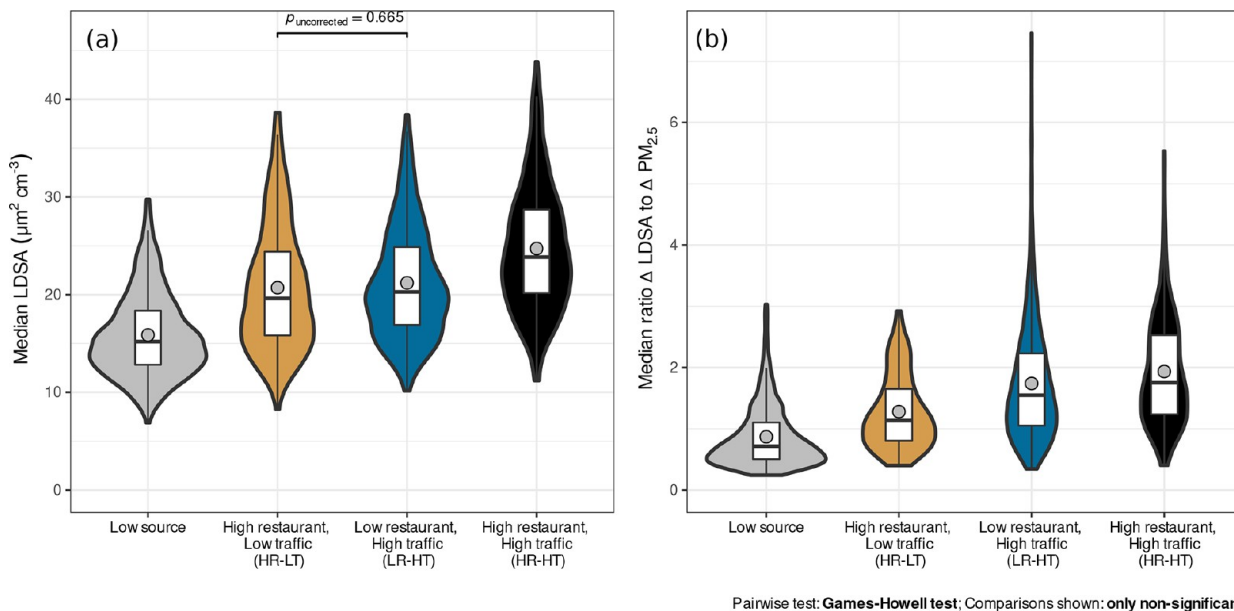


**Figure 5.** Box-and-violin plot showing, within each source category, distributions of gridded campaign median values of (a) LDSA concentrations and (b)  $\Delta \text{LDSA} / \Delta \text{PM}_{2.5}$  in units of  $(\mu\text{m}^2 \text{cm}^{-3}) / (\mu\text{g m}^{-3})$ . These plots are prepared using the *ggstatsplot* package in R,<sup>78</sup> which performs pairwise null hypothesis tests. Only the pairs for which the null hypothesis cannot be rejected (i.e.,  $p$  value  $> 0.05$ ) are tagged with their  $p$  value. In this case, for absolute LDSA concentrations, the HR-LT and LR-HT groups are found to be similar while all other combinations are statistically different from each other. For  $\Delta \text{LDSA} / \Delta \text{PM}_{2.5}$ , all groups are statistically different from each other.

have a surface area to volume ratio higher than that of larger cooking emission particles (section S1).

## ■ IMPLICATIONS

In this study, we characterized spatial patterns of particulate matter in central London by performing repeated mobile measurements of lung-deposited surface area (LDSA),  $\text{PM}_{2.5}$ , black carbon (BC), and  $\text{NO}_2$  from September 2018 to October 2019. Our measurements were predominantly performed from 5 a.m. to 11 p.m. on weekdays (section S4) and thus should not be compared directly against regulatory standards. Other limitations of this study are outlined in section S14.

We showed that the typical LDSA levels in London are more similar to previously reported urban background measurements in Leicester ( $22 \mu\text{m}^2 \text{cm}^{-3}$ ) and Zürich ( $19 \mu\text{m}^2 \text{cm}^{-3}$ )<sup>48,53</sup> than to more polluted areas such as Barcelona ( $37 \mu\text{m}^2 \text{cm}^{-3}$ ),<sup>49</sup> Lisbon ( $34 \mu\text{m}^2 \text{cm}^{-3}$ ),<sup>69</sup> and Los Angeles ( $53 \mu\text{m}^2 \text{cm}^{-3}$ ).<sup>52</sup> We showed persistently increased concentrations of LDSA in several parts of central London such as on major roadways and in commercial neighborhoods with a high number of restaurants. Recent literature and emission inventories show that cooking emissions from restaurants have neighborhood-scale impacts on air quality,<sup>20,79</sup> with PM contributions comparable to that from vehicular exhaust.<sup>18,42</sup> We hypothesized that our observed hot spots of LDSA concentrations, both absolute and background-subtracted ( $\Delta$ ), in commercial neighborhoods can be partly attributed to the dense presence of restaurants there. We confirmed this hypothesis using multiple lines of evidence. First, the campaign median concentrations in commercial neighborhoods are higher during peak meal preparation times (midday and evening). Second, we use campaign median emission ratios between LDSA and traffic markers (BC and  $\text{NO}_2$ ) to show that  $\Delta \text{LDSA} / \Delta \text{BC}$  and  $\Delta \text{LDSA} / \Delta \text{NO}_2$  are higher in commercial neighborhoods than on major roadways, indicating the presence of nonvehicular emission sources.

Third, we use geographic indicators of traffic and cooking emissions (major roadways and restaurants) to show quantitatively that both proxies are determinants of high LDSA concentrations. Fourth, while our measurements of  $\text{PM}_{2.5}$  using optical particle counting (particles smaller than  $\sim 180 \text{ nm}$  not detected) do not effectively capture the fresh vehicular exhaust emissions on major roadways, we do observe higher  $\text{PM}_{2.5}$  concentrations (both absolute and  $\Delta$ ) in commercial neighborhoods, further demonstrating the impact of cooking emissions, which typically contain 100–400 nm diameter particles.<sup>4,9</sup>

More scientific attention is being paid to the characterization of spatial and temporal patterns, determinants, sources, and health effects of ultrafine particles (UFPs). Recently, Apte et al.<sup>74</sup> found  $\text{NO}_x$  and particle number concentration to be moderately correlated in high-traffic areas of the San Francisco Bay area but found this correlation to significantly worsen in low-traffic areas. They attributed this behavior to new particle formation, especially during high insolation periods. While this is a reasonable conclusion, our analyses of interpollutant emission ratios show that in low-traffic areas with a high restaurant density, cooking emissions can also play an important role in enhancing particle concentrations without proportionally enhancing other species like  $\text{NO}_2$  and BC. While we relied on correlations (or lack thereof) among LDSA,  $\text{PM}_{2.5}$ ,  $\text{NO}_2$ , and BC to distinguish vehicular from nonvehicular emissions, other external measurements can also be used to more clearly identify cooking emissions. For instance, cooking emissions have been shown to emit volatile organic compounds such as aldehydes.<sup>80,81</sup> Collocated measurements of volatile organics performed in addition to species such as  $\text{PM}_{2.5}$ , LDSA, BC, etc., can thus aid in identifying some hot spots as not only nonvehicular but also specifically cooking-influenced. It should also be noted that our measurements, performed on street center lines, would be expected to be impacted more strongly by the immediately adjacent vehicular

emissions than by the more distant restaurant exhaust sources. As a result, the nonvehicular particulate matter concentrations breathed by pedestrians on pavements or sidewalks would likely be higher than those captured in our mobile sampling data set.

While a vast majority of high-spatial-resolution monitoring studies have measured pollutants such as NO, NO<sub>2</sub>, BC, and PM mass, a particular novelty of this study is the measurement of LDSA, the concentration of particles that could have the most serious health consequences.<sup>6,40,82</sup> We believe the methods and findings presented in this study are of timely importance to global efforts in urban hyperlocal air quality mapping, source apportionment, exposure assessment, and pollution alleviation. On September 22, 2021, the World Health Organization revised their guideline for healthy annual average PM<sub>2.5</sub> concentration from 10 to 5  $\mu\text{g m}^{-3}$ . A very small fraction of the global population lives in areas where this revised guideline is met.<sup>83</sup> As more attention is paid to urban air quality alleviation (e.g., California's Air Resources Board's Community Air Protection Program, focusing on criteria and toxic air pollutants from nonvehicular sources, and their impact on air quality at the community scale), studies such as ours can aid policymakers in designing urban air quality management strategies and urban planning that address important emission sources, vehicular and nonvehicular alike. Our study demonstrates the value of using high-spatial-resolution, neighborhood-scale monitoring of particle surface concentrations to inform concentrations of health-relevant components of particulate matter.

## ASSOCIATED CONTENT

### Supporting Information

The Supporting Information is available free of charge at <https://pubs.acs.org/doi/10.1021/acs.est.2c08096>.

Simulated particle size distributions; data quality assurance methods (instrument precision and MDL quantitation); local enhancement identification; temporal biases and seasonal artifacts; sampling uncertainty estimation; example time series of mobile sampling; diurnally stratified LDSA maps; local enhancement maps for PM<sub>2.5</sub>, BC, and NO<sub>2</sub>; probability of exceedance maps for PM<sub>2.5</sub>; gridded land-use classification; gridded pollutant concentrations, enhancements, and enhancement ratios; and a summary of assumptions and limitations of this study ([PDF](#))

## AUTHOR INFORMATION

### Corresponding Author

Rishabh U. Shah — Environmental Defense Fund, Austin, Texas 78701, United States; Present Address: Aclima, Inc., 10 Lombard St., Suite 300, San Francisco, CA 94111; [orcid.org/0000-0002-4608-1972](https://orcid.org/0000-0002-4608-1972); Email: [rshah6192@gmail.com](mailto:rshah6192@gmail.com)

### Authors

Lauren E. Padilla — Environmental Defense Fund, Austin, Texas 78701, United States

Daniel R. Peters — Environmental Defense Fund, Austin, Texas 78701, United States

Megan Dupuy-Todd — Environmental Defense Fund, Austin, Texas 78701, United States; Present Address: Clean Air Task Force, 114 State St., 6th Floor, Boston, MA 02109.

Elizabeth R. Fonseca — Environmental Defense Fund Europe, London EC3M 1DT, U.K.; Present Address: Centre for Environmental Policy, Imperial College London, London SW7 2AZ, U.K.

Geoffrey Q. Ma — National Physical Laboratory, Teddington, Middlesex TW11 0LW, U.K.; Yusuf Hamied Department of Chemistry, University of Cambridge, Cambridge CB2 1EW, U.K.

Olakekan A. M. Popoola — Yusuf Hamied Department of Chemistry, University of Cambridge, Cambridge CB2 1EW, U.K.; [orcid.org/0000-0003-2390-8436](https://orcid.org/0000-0003-2390-8436)

Roderic L. Jones — Yusuf Hamied Department of Chemistry, University of Cambridge, Cambridge CB2 1EW, U.K.

Jim Mills — ACOEM UK Ltd., Tewkesbury GL20 8GD, U.K.

Nicholas A. Martin — National Physical Laboratory,

Teddington, Middlesex TW11 0LW, U.K.

Ramón A. Alvarez — Environmental Defense Fund, Austin, Texas 78701, United States

Complete contact information is available at:

<https://pubs.acs.org/10.1021/acs.est.2c08096>

### Notes

The authors declare no competing financial interest.

## ACKNOWLEDGMENTS

This work was supported by the Children's Investment Fund Foundation and the Clean Air Fund, and further funding support was provided by Signe Ostby and Scott Cook, Valhalla Foundation, and the High Meadows Foundation for a postdoctoral fellowship. The Breathe London pilot project was convened by C40 Cities and the Mayor of London. The authors are grateful for the dedication and skill of a team of Google Street View drivers (Glenroy Dalling, Adam Bennett, John Arnold, and Dwain Smith) and Operations staff (Nigel Timm, Ivo Furano, Stefan Baumann, Andrea Braun, Bryan White, and Evans Arabu). The authors thank William Hicklin for custom software and database development that synchronized the streaming and polling of data from many different instruments. The authors thank Stefan Bell, Idris Hayward, and Georgie Coppin at National Physical Laboratory and Karin Tuxen-Bettman at Google Earth Outreach for arranging and coordinating access to the mobile monitoring vehicles, instrumentation, and cloud data platform. The authors appreciate insightful discussions with Tammy Thompson, David Miller, Greg Slater, and Christopher Portier.

## REFERENCES

- (1) Understanding the Health Effects of Ambient Ultrafine Particles. Health Effects Institute: Boston, 2013 (<https://www.healtheffects.org/publication/understanding-health-effects-ambient-ultrafine-particles>).
- (2) Apte, J. S.; Marshall, J. D.; Cohen, A. J.; Brauer, M. Addressing Global Mortality from Ambient PM<sub>2.5</sub>. *Environ. Sci. Technol.* **2015**, *49*, 8057–8066.
- (3) London Health Burden of Current Air Pollution and Future Health Benefits of Mayoral Air Quality Policies. Imperial College: London, 2020 (<http://erg.ic.ac.uk/research/home/projects/tfl-hia-maqp.html>).
- (4) Ye, Q.; Gu, P.; Li, H. Z.; Robinson, E. S.; Lipsky, E.; Kaltsoudis, C.; Lee, A. K.; Apte, J. S.; Robinson, A. L.; Sullivan, R. C.; Presto, A. A.; Donahue, N. M. Spatial Variability of Sources and Mixing State of Atmospheric Particles in a Metropolitan Area. *Environ. Sci. Technol.* **2018**, *52*, 6807–6815.

- (5) Stölzel, M.; Breitner, S.; Cyrys, J.; Pitz, M.; Wölke, G.; Kreyling, W.; Heinrich, J.; Wichmann, H. E.; Peters, A. Daily mortality and particulate matter in different size classes in Erfurt, Germany. *J. Exposure Sci. Environ. Epidemiol.* **2007**, *17*, 458–467.
- (6) Oberdörster, G. Toxicology of ultrafine particles: in vivo studies. *Philos. Trans. R. Soc., A* **2000**, *358*, 2719–2740.
- (7) Möller, W.; Felten, K.; Sommerer, K.; Scheuch, G.; Meyer, G.; Meyer, P.; Haussinger, K.; Kreyling, W. G. Deposition, retention, and translocation of ultrafine particles from the central airways and lung periphery. *Am. J. Respir. Crit. Care Med.* **2008**, *177*, 426–432.
- (8) Nemmar, A.; Hoet, P.; Vanquickenborne, B.; Dinsdale, D.; Thomeer, M.; Hoylaerts, M.; Vanbilloen, H.; Mortelmans, L.; Nemery, B. Passage of Inhaled Particles Into the Blood Circulation in Humans. *Circulation* **2002**, *105*, 411–414.
- (9) Ye, Q.; Li, H. Z.; Gu, P.; Robinson, E. S.; Apte, J. S.; Sullivan, R. C.; Robinson, A. L.; Donahue, N. M.; Presto, A. A. Moving beyond Fine Particle Mass: High-Spatial Resolution Exposure to Source-Resolved Atmospheric Particle Number and Chemical Mixing State. *Environ. Health Perspect.* **2020**, *128*, 017009.
- (10) Apte, J. S.; Kirchstetter, T. W.; Reich, A. H.; Deshpande, S. J.; Kaushik, G.; Chel, A.; Marshall, J. D.; Nazaroff, W. W. Concentrations of fine, ultrafine, and black carbon particles in auto-rickshaws in New Delhi, India. *Atmos. Environ.* **2011**, *45*, 4470–4480.
- (11) Zhang, K. M.; Wexler, A. S. Evolution of particle number distribution near roadways - Part I: Analysis of aerosol dynamics and its implications for engine emission measurement. *Atmos. Environ.* **2004**, *38*, 6643–6653.
- (12) Saha, P. K.; Zimmerman, N.; Malings, C.; Hauryliuk, A.; Li, Z.; Snell, L.; Subramanian, R.; Lipsky, E.; Apte, J. S.; Robinson, A. L.; Presto, A. A. Quantifying high-resolution spatial variations and local source impacts of urban ultrafine particle concentrations. *Sci. Total Environ.* **2019**, *655*, 473–481.
- (13) Karner, A. A.; Eisinger, D. S.; Niemeier, D. A. Near-roadway air quality: Synthesizing the findings from real-world data. *Environ. Sci. Technol.* **2010**, *44*, 5334–5344.
- (14) Shah, R. U.; Robinson, E. S.; Gu, P.; Apte, J. S.; Marshall, J. D.; Robinson, A. L.; Presto, A. A. Socio-economic disparities in exposure to urban restaurant emissions are larger than for traffic. *Environ. Res. Lett.* **2020**, *15*, 114039.
- (15) Canagaratna, M. R.; Onasch, T. B.; Wood, E. C.; Herndon, S. C.; Jayne, J. T.; Cross, E. S.; Miake-Lye, R. C.; Kolb, C. E.; Worsnop, D. R. Evolution of Vehicle Exhaust Particles in the Atmosphere. *J. Air Waste Manage. Assoc.* **2010**, *60*, 1192–1203.
- (16) Saha, P. K.; Khlystov, A.; Snyder, M. G.; Grieshop, A. P. Characterization of air pollutant concentrations, fleet emission factors, and dispersion near a North Carolina interstate freeway across two seasons. *Atmos. Environ.* **2018**, *177*, 143–153.
- (17) Apte, J. S.; Messier, K. P.; Gani, S.; Brauer, M.; Kirchstetter, T. W.; Lunden, M. M.; Marshall, J. D.; Portier, C. J.; Vermeulen, R. C.; Hamburg, S. P. High-Resolution Air Pollution Mapping with Google Street View Cars: Exploiting Big Data. *Environ. Sci. Technol.* **2017**, *51*, 6999–7008.
- (18) Shah, R. U.; Robinson, E. S.; Gu, P.; Robinson, A.; Apte, J. S.; Presto, A. A. High-spatial-resolution mapping and source apportionment of aerosol composition in Oakland, California using mobile aerosol mass spectrometry. *Atmospheric Chemistry and Physics* **2018**, *18*, 16325–16344.
- (19) Miller, D. J.; Actkinson, B.; Padilla, L.; Griffin, R. J.; Moore, K.; Lewis, P. G. T.; Gardner-Frolick, R.; Craft, E.; Portier, C. J.; Hamburg, S. P.; Alvarez, R. A. Characterizing Elevated Urban Air Pollutant Spatial Patterns with Mobile Monitoring in Houston, Texas. *Environ. Sci. Technol.* **2020**, *54*, 2133–2142.
- (20) Robinson, E. S.; Gu, P.; Ye, Q.; Li, H. Z.; Shah, R. U.; Apte, J. S.; Robinson, A. L.; Presto, A. A. Restaurant Impacts on Outdoor Air Quality: Elevated Organic Aerosol Mass from Restaurant Cooking with Neighborhood-Scale Plume Extents. *Environ. Sci. Technol.* **2018**, *52*, 9285–9294.
- (21) Chambliss, S. E.; Preble, C. V.; Caubel, J. J.; Cados, T.; Messier, K. P.; Alvarez, R. A.; LaFranchi, B.; Lunden, M.; Marshall, J. D.; Szpiro, A. A.; Kirchstetter, T. W.; Apte, J. S. Comparison of Mobile and Fixed-Site Black Carbon Measurements for High-Resolution Urban Pollution Mapping. *Environ. Sci. Technol.* **2020**, *54*, 7848–7857.
- (22) Li, H. Z.; Dallmann, T. R.; Gu, P.; Presto, A. A. Application of mobile sampling to investigate spatial variation in fine particle composition. *Atmos. Environ.* **2016**, *142*, 71–82.
- (23) Li, H. Z.; Dallmann, T. R.; Li, X.; Gu, P.; Presto, A. A. Urban organic aerosol exposure: Spatial variations in composition and source impacts. *Environ. Sci. Technol.* **2018**, *52*, 415–426.
- (24) Giordano, M. R.; Malings, C.; Pandis, S. N.; Presto, A. A.; McNeill, F.; Westervelt, D. M.; Beekmann, M.; Subramanian, R. From low-cost sensors to high-quality data: A summary of challenges and best practices for effectively calibrating low-cost particulate matter mass sensors. *J. Aerosol Sci.* **2021**, *158*, 105833.
- (25) An update on low-cost sensors for the measurement of atmospheric composition. World Meteorological Organization: Geneva, 2020 ([https://library.wmo.int/doc\\_num.php?explnum\\_id=10620](https://library.wmo.int/doc_num.php?explnum_id=10620)).
- (26) Desouza, P. N.; Oriama, P. A.; Pedersen, P. P.; Horstmann, S.; Gordillo-Dagallier, L.; Christensen, C. N.; Franck, C. O.; Ayah, R.; Kahn, R. A.; Klopp, J. M.; Messier, K. P.; Kinney, P. L. Spatial variation of fine particulate matter levels in Nairobi before and during the covid-19 curfew: Implications for environmental justice. *Environ. Res. Commun.* **2021**, *3*, 071003.
- (27) Sinaga, D.; Setyawati, W.; Cheng, F. Y.; Lung, S. C. C. Investigation on daily exposure to PM<sub>2.5</sub> in Bandung city, Indonesia using low-cost sensor. *J. Exposure Sci. Environ. Epidemiol.* **2020**, *30*, 1001–1012.
- (28) Subramanian, R. Air pollution in Kigali, Rwanda: spatial and temporal variability, source contributions, and the impact of car-free Sundays. *Tydskr. Skoon Lug* **2020**, *30*, 1–15.
- (29) Morawska, L.; Thai, P. K.; Liu, X.; Asumadu-Sakyi, A.; Ayoko, G.; Bartanova, A.; Bedini, A.; Chai, F.; Christensen, B.; Dunbabin, M.; Gao, J.; Hagler, G. S.; Jayaratne, R.; Kumar, P.; Lau, A. K.; Louie, P. K.; Mazaheri, M.; Ning, Z.; Motta, N.; Mullins, B.; Rahman, M. M.; Ristovski, Z.; Shafiei, M.; Tjondronegoro, D.; Westerdahl, D.; Williams, R. Applications of low-cost sensing technologies for air quality monitoring and exposure assessment: How far have they gone? *Environ. Int.* **2018**, *116*, 286–299.
- (30) Singh, A.; Ng'ang'a, D.; Gatari, M. J.; Kidane, A. W.; Alemu, Z. A.; Derrick, N.; Webster, M. J.; Bartington, S. E.; Thomas, G. N.; Avis, W.; Pope, F. D. Air quality assessment in three east african cities using calibrated low-cost sensors with a focus on road-based hotspots. *Environ. Res. Commun.* **2021**, *3*, 075007.
- (31) Aguiar, E. F. K.; Roig, H. L.; Mancini, L. H.; de Carvalho, E. N. C. B. Low-Cost Sensors Calibration for Monitoring Air Quality in the Federal District - Brazil. *J. Environ. Prot.* **2015**, *06*, 173–189.
- (32) Malings, C.; Westervelt, D. M.; Hauryliuk, A.; Presto, A. A.; Grieshop, A.; Bittner, A.; Beekmann, M. Application of low-cost fine particulate mass monitors to convert satellite aerosol optical depth to surface concentrations in North America and Africa. *Atmos. Meas. Tech.* **2020**, *13*, 3873–3892.
- (33) Zheng, T.; Bergin, M. H.; Johnson, K. K.; Tripathi, S. N.; Shirodkar, S.; Landis, M. S.; Sutaria, R.; Carlson, D. E. Field evaluation of low-cost particulate matter sensors in high-and low-concentration environments. *Atmospheric Measurement Techniques* **2018**, *11*, 4823–4846.
- (34) Wang, Y.; Li, J.; Jing, H.; Zhang, Q.; Jiang, J.; Biswas, P. Laboratory Evaluation and Calibration of Three Low-Cost Particle Sensors for Particulate Matter Measurement. *Aerosol Sci. Technol.* **2015**, *49*, 1063–1077.
- (35) He, M.; Kuerbanjiang, N.; Dhaniyala, S. Performance characteristics of the low-cost Plantower PMS optical sensor. *Aerosol Sci. Technol.* **2020**, *54*, 232–241.
- (36) Abernethy, R. C.; Allen, R. W.; McKendry, I. G.; Brauer, M. A land use regression model for ultrafine particles in Vancouver, Canada. *Environ. Sci. Technol.* **2013**, *47*, 5217–5225.

- (37) Presto, A. A.; Saha, P. K.; Robinson, A. L. Past, present, and future of ultrafine particle exposures in North America. *Atmospheric Environment: X* **2021**, *10*, 100109.
- (38) Choi, W.; Ranasinghe, D.; Bunavage, K.; DeShazo, J. R.; Wu, L.; Seguel, R.; Winer, A. M.; Paulson, S. E. The effects of the built environment, traffic patterns, and micrometeorology on street level ultrafine particle concentrations at a block scale: Results from multiple urban sites. *Sci. Total Environ.* **2016**, *553*, 474–485.
- (39) Kim, J.-J.; Choi, W.; Paulson, S. E.; Ranasinghe, D.; DeShazo, J. Where to locate transit stops: Cross-intersection profiles of ultrafine particles and implications for pedestrian exposure. *Environ. Pollut.* **2018**, *233*, 235–245.
- (40) Donaldson, K.; Tran, L.; Jimenez, L. A.; Duffin, R.; Newby, D. E.; Mills, N.; MacNee, W.; Stone, V. Combustion-derived nanoparticles: A review of their toxicology following inhalation exposure. *Particle and Fibre Toxicology* **2005**, *2*, 1–14.
- (41) Maier, K. L.; Alessandrini, F.; Beck-Speier, I.; Josef Hofer, T. P.; Diabaté, S.; Bitterle, E.; Stöger, T.; Jakob, T.; Behrendt, H.; Horsch, M.; Beckers, J.; Ziesenis, A.; Hültner, L.; Frankenberger, M.; Krauss-Etschmann, S.; Schulz, H. Health Effects of Ambient Particulate Matter—Biological Mechanisms and Inflammatory Responses to In Vitro and In Vivo Particle Exposures. *Inhalation Toxicol.* **2008**, *20*, 319–337.
- (42) Gu, P.; Li, H. Z.; Ye, Q.; Robinson, E. S.; Apte, J. S.; Robinson, A. L.; Presto, A. A. Intracity Variability of Particulate Matter Exposure Is Driven by Carbonaceous Sources and Correlated with Land-Use Variables. *Environ. Sci. Technol.* **2018**, *52*, 11545–11554.
- (43) Zhao, B.; Yu, L.; Wang, C.; Shuai, C.; Zhu, J.; Qu, S.; Taiebat, M.; Xu, M. Urban Air Pollution Mapping Using Fleet Vehicles as Mobile Monitors and Machine Learning. *Environ. Sci. Technol.* **2021**, *55*, 5579–5588.
- (44) Wu, Y.; Wang, Y.; Wang, L.; Song, G.; Gao, J.; Yu, L. Application of a taxi-based mobile atmospheric monitoring system in Cangzhou, China. *Transportation Research Part D: Transport and Environment* **2020**, *86*, 102449.
- (45) Li, H. Z.; Gu, P.; Ye, Q.; Zimmerman, N.; Robinson, E. S.; Subramanian, R.; Apte, J. S.; Robinson, A. L.; Presto, A. A. Spatially dense air pollutant sampling: Implications of spatial variability on the representativeness of stationary air pollutant monitors. *Atmospheric Environment: X* **2019**, *2*, 100012.
- (46) Simon, M. C.; Patton, A. P.; Naumova, E. N.; Levy, J. I.; Kumar, P.; Brugge, D.; Durant, J. L. Combining Measurements from Mobile Monitoring and a Reference Site to Develop Models of Ambient Ultrafine Particle Number Concentration at Residences. *Environ. Sci. Technol.* **2018**, *52*, 6985–6995.
- (47) Hennig, F.; Quass, U.; Hellack, B.; Küpper, M.; Kuhlbusch, T. A. J.; Stafoviggia, M.; Hoffmann, B. Ultrafine and Fine Particle Number and Surface Area Concentrations and Daily Cause-Specific Mortality in the Ruhr Area, Germany, 2009–2014. *Environ. Health Perspect.* **2018**, *126*, 027008.
- (48) Hama, S. M.; Ma, N.; Cordell, R. L.; Kos, G. P.; Wiedensohler, A.; Monks, P. S. Lung deposited surface area in Leicester urban background site/UK: Sources and contribution of new particle formation. *Atmos. Environ.* **2017**, *151*, 94–107.
- (49) Reche, C.; Viana, M.; Brines, M.; Pérez, N.; Beddows, D.; Alastuey, A.; Querol, X. Determinants of aerosol lung-deposited surface area variation in an urban environment. *Science of The Total Environment* **2015**, *517*, 38–47.
- (50) Kuula, J.; Kuuluvainen, H.; Niemi, J. V.; Saukko, E.; Portin, H.; Kousa, A.; Aurela, M.; Rönkkö, T.; Timonen, H. Long-term sensor measurements of lung deposited surface area of particulate matter emitted from local vehicular and residential wood combustion sources. *Aerosol Sci. Technol.* **2020**, *54*, 190–202.
- (51) Bousiotis, D.; Singh, A.; Haugen, M.; Beddows, D. C.; Diez, S.; Murphy, K. L.; Edwards, P. M.; Boies, A.; Harrison, R. M.; Pope, F. D. Assessing the sources of particles at an urban background site using both regulatory instruments and low-cost sensors – a comparative study. *Atmospheric Measurement Techniques* **2021**, *14*, 4139–4155.
- (52) Ntziachristos, L.; Polidori, A.; Phuleria, H.; Geller, M. D.; Sioutas, C. Application of a diffusion charger for the measurement of particle surface concentration in different environments. *Aerosol Sci. Technol.* **2007**, *41*, 571–580.
- (53) Fierz, M.; Houle, C.; Steigmeier, P.; Burtscher, H. Design, calibration, and field performance of a miniature diffusion size classifier. *Aerosol Sci. Technol.* **2011**, *45*, 1–10.
- (54) Padilla, L. E.; Ma, G. Q.; Peters, D.; Dupuy-Todd, M.; Forsyth, E.; Stidworthy, A.; Mills, J.; Bell, S.; Hayward, I.; Coppin, G.; Moore, K.; Fonseca, E.; Popoola, O. A.; Douglas, F.; Slater, G.; Tuxen-Bettman, K.; Carruthers, D.; Martin, N. A.; Jones, R. L.; Alvarez, R. A. New methods to derive street-scale spatial patterns of air pollution from mobile monitoring. *Atmos. Environ.* **2022**, *270*, 118851.
- (55) Peters, D. R.; Popoola, O. A.; Jones, R. L.; Martin, N. A.; Mills, J.; Fonseca, E. R.; Stidworthy, A.; Forsyth, E.; Carruthers, D.; Dupuy-Todd, M.; Douglas, F.; Moore, K.; Shah, R. U.; Padilla, L. E.; Alvarez, R. A. Evaluating uncertainty in sensor networks for urban air pollution insights. *Atmospheric Measurement Techniques* **2022**, *15*, 321–334.
- (56) Ku, B. K.; Kulkarni, P. Comparison of diffusion charging and mobility-based methods for measurement of aerosol agglomerate surface area. *J. Aerosol Sci.* **2012**, *47*, 100–110.
- (57) Pandis, S. N.; Baltensperger, U.; Wolfenbarger, J. K.; Seinfeld, J. H. Inversion of aerosol data from the epiphanometer. *J. Aerosol Sci.* **1991**, *22*, 417–428.
- (58) Gomes, J.; Albuquerque, P.; Esteves, H. M. D. S.; Carvalho, P. A. Notice on a methodology for characterizing emissions of ultrafine particles/nanoparticles in microenvironments. *Energy and Emission Control Technologies* **2013**, *2013*, 15–27.
- (59) Fissan, H.; Neumann, S.; Trampe, A.; Pui, D. Y.; Shin, W. G. Rationale and principle of an instrument measuring lung deposited nanoparticle surface area. *J. Nanopart. Res.* **2006**, *9*, 53–59.
- (60) Evaluation of the Ambient Air Particulate Matter Test Reports Submitted for Approval and Certification within the MCERTS Scheme for UK Particulate Matter. Environmental Agency, 2016 (<https://www.csagroupuk.org/wp-content/uploads/2016/04/MCERTSCCPMT6PALASPM10PM2.5V10.4.pdf>).
- (61) Sun, Y.; Xu, W.; Zhang, Q.; Jiang, Q.; Canonaco, F.; Prévôt, A. S. H.; Fu, P.; Li, J.; Jayne, J.; Worsnop, D. R.; Wang, Z. Source apportionment of organic aerosol from 2-year highly time-resolved measurements by an aerosol chemical speciation monitor in Beijing, China. *Atmospheric Chemistry and Physics* **2018**, *18*, 8469–8489.
- (62) Brantley, H. L.; Hagler, G. S. W.; Kimbrough, E. S.; Williams, R. W.; Mukerjee, S.; Neas, L. M. Mobile air monitoring data-processing strategies and effects on spatial air pollution trends. *Atmospheric Measurement Techniques* **2014**, *7*, 2169–2183.
- (63) Zhao, J.; Qiu, Y.; Zhou, W.; Xu, W.; Wang, J.; Zhang, Y. Organic Aerosol Processing During Winter Severe Haze Episodes in Beijing. *J. Geophys. Res.: Atmos.* **2019**, *124*, 10248.
- (64) Zhao, J.; Du, W.; Zhang, Y.; Wang, Q.; Chen, C.; Xu, W.; Han, T.; Wang, Y.; Fu, P.; Wang, Z.; Li, Z.; Sun, Y. Insights into aerosol chemistry during the 2015 China Victory Day parade: Results from simultaneous measurements at ground level and 260 g cm<sup>-3</sup> in Beijing. *Atmospheric Chemistry and Physics* **2017**, *17*, 3215–3232.
- (65) Hagler, G. S. W.; Yelverton, T. L. B.; Vedantham, R.; Hansen, A. D. A.; Turner, J. R. Post-processing method to reduce noise while preserving high time resolution in aethalometer real-time black carbon data. *Aerosol and Air Quality Research* **2011**, *11*, 539–546.
- (66) Messier, K. P.; Chambliss, S. E.; Gani, S.; Alvarez, R.; Brauer, M.; Choi, J. J.; Hamburg, S. P.; Kerckhoff, J.; Lafranchi, B.; Lunden, M. M.; Marshall, J. D.; Portier, C. J.; Roy, A.; Szapiro, A. A.; Vermeulen, R. C.; Apte, J. S. Mapping Air Pollution with Google Street View Cars: Efficient Approaches with Mobile Monitoring and Land Use Regression. *Environ. Sci. Technol.* **2018**, *52*, 12563–12572.
- (67) Dallmann, T. R.; Harley, R. A.; Kirchstetter, T. W. Effects of diesel particle filter retrofits and accelerated fleet turnover on drayage truck emissions at the port of Oakland. *Environ. Sci. Technol.* **2011**, *45*, 10773–10779.
- (68) Dallmann, T. R.; Kirchstetter, T. W.; DeMartini, S. J.; Harley, R. A. Quantifying On-Road Emissions from Gasoline-Powered Motor

- Vehicles: Accounting for the Presence of Medium- and Heavy-Duty Diesel Trucks. *Environ. Sci. Technol.* **2013**, *47*, 13873–13881.
- (69) Gomes, J. F. P.; Bordado, J. C. M.; Albuquerque, P. C. S. On the assessment of exposure to airborne ultrafine particles in urban environments. *Journal of Toxicology and Environmental Health - Part A: Current Issues* **2012**, *75*, 1316–1329.
- (70) Gietl, J. K.; Lawrence, R.; Thorpe, A. J.; Harrison, R. M. Identification of brake wear particles and derivation of a quantitative tracer for brake dust at a major road. *Atmos. Environ.* **2010**, *44*, 141–146.
- (71) Sanders, P. G.; Xu, N.; Dalka, T. M.; Maricq, M. M. Airborne brake wear debris: Size distributions, composition, and a comparison of dynamometer and vehicle tests. *Environ. Sci. Technol.* **2003**, *37*, 4060–4069.
- (72) Robinson, E. S.; Shah, R. U.; Messier, K.; Gu, P.; Li, H. Z.; Apte, J. S.; Robinson, A. L.; Presto, A. A. Land-Use Regression Modeling of Source-Resolved Fine Particulate Matter Components from Mobile Sampling. *Environ. Sci. Technol.* **2019**, *53*, 8925–8937.
- (73) Vert, C.; Meliefste, K.; Hoek, G. Outdoor ultrafine particle concentrations in front of fast food restaurants. *J. Exposure Sci. Environ. Epidemiol.* **2016**, *26*, 35–41.
- (74) Apte, J.; Gani, S.; Chambliss, S.; Messier, K.; Lunden, M. Potential underestimation of ultrafine particle exposure when using proxy pollutants. *Environmental Epidemiology* **2019**, *3*, 13–14.
- (75) Ultrafine Particles (UFP) in the UK. Air Quality Expert Group (AQEG) of the Department for Environment, Food and Rural Affairs (Defra): London, 2018 ([https://uk-air.defra.gov.uk/assets/documents/reports/cat09/1807261113\\_180703\\_UFP\\_Report\\_FINAL\\_for\\_publication.pdf](https://uk-air.defra.gov.uk/assets/documents/reports/cat09/1807261113_180703_UFP_Report_FINAL_for_publication.pdf)).
- (76) Jones, A. M.; Harrison, R. M.; Barratt, B.; Fuller, G. A large reduction in airborne particle number concentrations at the time of the introduction of “sulphur free” diesel and the London Low Emission Zone. *Atmos. Environ.* **2012**, *50*, 129–138.
- (77) Lepistö, T.; Kuuluvainen, H.; Lintusaari, H.; Kuittinen, N.; Salo, L.; Helin, A.; Niemi, J. V.; Manninen, H. E.; Timonen, H.; Jalava, P.; Saarikoski, S.; Rönkkö, T. Connection between lung deposited surface area (LDSA) and black carbon (BC) concentrations in road traffic and harbour environments. *Atmos. Environ.* **2022**, *272*, 118931.
- (78) Patil, I. Visualizations with statistical details: The ‘ggstatsplot’ approach. *Journal of Open Source Software* **2021**, *6*, 3167.
- (79) London Atmospheric Emissions Inventory (LAEI). 2019 (<https://data.london.gov.uk/air-quality/>) (accessed 2022-12-03).
- (80) Mountaz, S.; Percival, B. C.; Parmar, D.; Grootveld, K. L.; Jansson, P.; Grootveld, M. Toxic aldehyde generation in and food uptake from culinary oils during frying practices: peroxidative resistance of a monounsaturated-rich algae oil. *Sci. Rep.* **2019**, *9*, 1–21.
- (81) Katragadda, H. R.; Fullana, A.; Sidhu, S.; Carbonell-Barrachina, A. A. Emissions of volatile aldehydes from heated cooking oils. *Food Chem.* **2010**, *120*, 59–65.
- (82) Donaldson, K.; Li, X. Y.; MacNee, W. Ultrafine (nanometre) particle mediated lung injury. *J. Aerosol Sci.* **1998**, *29*, 553–560.
- (83) Hammer, M. S.; Van Donkelaar, A.; Li, C.; Lyapustin, A.; Sayer, A. M.; Hsu, N. C.; Levy, R. C.; Garay, M. J.; Kalashnikova, O. V.; Kahn, R. A.; Brauer, M.; Apte, J. S.; Henze, D. K.; Zhang, L.; Zhang, Q.; Ford, B.; Pierce, J. R.; Martin, R. V. Global Estimates and Long-Term Trends of Fine Particulate Matter Concentrations (1998–2018). *Environ. Sci. Technol.* **2020**, *54*, 7879–7890.

## □ Recommended by ACS

### Investigating Use of Low-Cost Sensors to Increase Accuracy and Equity of Real-Time Air Quality Information

Ellen M. Considine, Priyanka deSouza, *et al.*

JANUARY 09, 2023

ENVIRONMENTAL SCIENCE & TECHNOLOGY

READ ▾

### Vapors Are Lost to Walls, Not to Particles on the Wall: Artifact-Corrected Parameters from Chamber Experiments and Implications for Global Secondary Organic Aerosol

Kelsey R. Bilsback, Shantanu H. Jathar, *et al.*

DECEMBER 23, 2022

ENVIRONMENTAL SCIENCE & TECHNOLOGY

READ ▾

### Influence of Wildfire on Urban Ozone: An Observationally Constrained Box Modeling Study at a Site in the Colorado Front Range

Pamela S. Rickly, Steven S. Brown, *et al.*

JANUARY 06, 2023

ENVIRONMENTAL SCIENCE & TECHNOLOGY

READ ▾

### Reaction of HOCl with Wood Smoke Aerosol: Impacts on Indoor Air Quality and Outdoor Reactive Chlorine

Spiro D. Jorga, Jonathan P. D. Abbott, *et al.*

JANUARY 06, 2023

ENVIRONMENTAL SCIENCE & TECHNOLOGY

READ ▾

Get More Suggestions >